Available online at www.sciencedirect.com
SCIENCE DIRECT®
Journal of Power Sources 123 (2003) 17–25
JOURNAL OF POWER SOURCES
www.elsevier.com/locate/jpowsour

Identification of O_2 reduction processes at yttria stabilized zirconia|doped lanthanum manganite interface

X.J. Chen, K.A. Khor*, S.H. Chan

Fuel Cell Strategic Research Program, School of Mechanical and Production Engineering, Nanyang Technological University, 50 Nanyang Avenue, Singapore 639798, Singapore

Received 27 January 2003; accepted 6 March 2003

Abstract

Oxygen reduction processes at a yttria stabilized zirconia|doped lanthanum manganite (LSM|YSZ) interface are investigated by ac impedance spectroscopy. Three semi-arcs are clearly observed at an oxygen partial pressure (p_{O_2}) of 0.001 atm. The constant-phase element of frequency arc and the p_{O_2}-dependence of $1/R$ (R: resistance) are correlated to interpret the reaction processes associated with the frequency arcs. It is found that at least five elementary steps are involved in oxygen reduction at the LSM|YSZ interface. Three of these steps are identified as the rate-determining steps, namely: (i) gas diffusion through the porous LSM electrode from the bulk to the reaction sites; (ii) surface diffusion of oxygen intermediate species along the LSM surface; (iii) incorporation of oxygen ions from the three phase boundary into the YSZ electrolyte lattice. The p_{O_2}-dependent exchange current density of the rate-determining step predicted by model is consistent with the experimental data, which further confirms the validity of the proposed oxygen reduction processes at the LSM|YSZ interface.

Keywords: Powders-solid state reaction; Impedance; Perovskites; Fuel cells

1. Introduction

Strontium doped lanthanum manganite ($La_{1-x}Sr_xMnO_3$, LSM) is widely used in solid oxide fuel cells (SOFCs) as the cathode material because of its high electrochemical activity for oxygen reduction as well as its thermal compatibility and chemical stability with yttria stabilized zirconia (YSZ) electrolyte [1,2]. The oxygen reduction on the LSM surface involves a complex reaction mechanism. Electrochemical impedance spectroscopy (EIS) is a powerful method that can be employed to investigate the reaction mechanisms. In the Nyquist plot, the impedance of the LSM cathode is composed of a series of overlapping arcs, which reflect the electrochemical, physical and chemical processes of oxygen reduction on the LSM surface. Impedance spectroscopy is a very sensitive measurement technique; any small variations can affect the impedance spectra. Differences in LSM composition [3,4], sintering temperature [5,6], cathode polarization [7] and gas composition [8] will result in different LSM surface conditions, and thus will affect the impedance spectra. Although many studies have been undertaken to understand oxygen reduction processes at the LSM|YSZ interface, inconsistencies were found in literature. The various reports have claimed that the rate-determining step ranges from charge-transfer reaction [9], dissociation and adsorption of oxygen on the LSM surface [5,10], oxygen diffusion through the porous LSM electrode at low oxygen partial pressure or high overpotential [11], to the surface diffusion of oxygen intermediate species [12–14].

Elucidation of the oxygen reduction processes at the LSM|YSZ interface is based on resolving of the overlapping arcs of the impedance spectra. In actual conditions, however, it is difficult to separate adequately the overlapping arcs, which have been reported to consist of one to three depressed arcs [11,15]. In this study, a series of experiments have been carried out at different experimental conditions, i.e. temperature, oxygen partial pressure and overpotential, to interpret O_2 reduction processes at the YSZ|LSM interface. The constant-phase element (or double-layer capacitor) is used to determine whether the impedance frequency arc is an electrochemical or chemical process. The possible oxygen species on the LSM surface involved in oxygen reduction are discussed and a model which considers electrochemical and chemical processes is proposed.

* Corresponding author. Fax: +65-6-7911859.
E-mail address: mkakhor@ntu.edu.sg (K.A. Khor).

0378-7753/$ – see front matter © 2003 Elsevier Science B.V. All rights reserved.
doi:10.1016/S0378-7753(03)00436-1

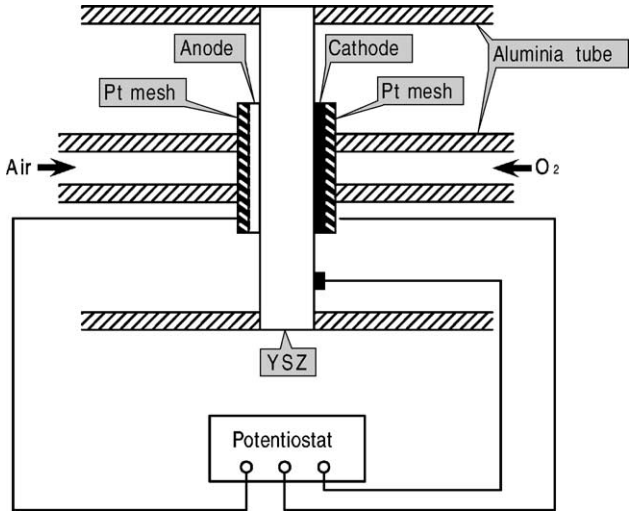

Fig. 1. Measurement circuit of three-electrode single fuel cell with potentiostat.

2. Experimental

The YSZ electrolyte was prepared from 8 mol% yttria stabilized zirconia powder (TZ8Y, Tosoh Corporation, Japan) by uniaxial pressing with pressure of 50 MPa, followed by sintering at 1500 °C for 2 h. $La_{0.85}Sr_{0.15}MnO_3$ powder (Nextech, USA) with a mean particle size of 1 μm was used as the raw material. The LSM electrode was applied to the YSZ electrolyte substrate by screen-printing and then sintered at 1150 °C for 2 h. The electrode thickness was around 50 μm and the electrode surface area was 0.785 cm^2. Platinum paste was coated on the other side of the YSZ substrate as the counter electrode and the reference electrode, followed by sintering at 1100 °C for 1 h. The distance between counter and reference electrode is ∼4 mm. The symmetrical configuration of the test cell is shown in Fig. 1. The counter and reference electrodes were exposed to the air and the LSM electrode was exposed to the balanced gas with different oxygen partial pressure. The newly prepared LSM electrode was initially polarized at 850 °C with a constant cathodic current of 300 mA cm^{-2} for 120 min before the electrochemical testing. The polarization was interrupted from time to time (2, 5, 30 and 120 min) to make the electrochemical impedance spectroscopy measurements. The effect of oxygen partial pressure and temperature on the impedance of the LSM electrode was investigated between 700 and 950 °C in increments of 50 °C, and at oxygen partial pressures of 0.001, 0.01, 0.21 and 1 atm.

3. Results and discussion

3.1. Microstructure of LSM electrode

The scanning electron micrograph of the cross-section of a newly prepared half-cell, i.e. YSZ electrolyte and LSM electrode interface, before and after 120 min of cathodic current/potential treatment is shown in Fig. 2. The microstructure and morphology of the LSM electrode are affected by the current/potential passage. Jiang and Love [16] have observed a similar variation of the microstructure of LSM electrode under cathodic polarization. The YSZ|LSM interface before cathodic current passage shows a flat-shape structure, which is an agglomeration of small LSM particles. After cathodic current treatment, the grains of the sphere-structure can be clearly observed in the electron micrograph. This may be due to the grain boundary migration of LSM grains during the passage of current. The coverage of the LSM electrode on the YSZ electrolyte will be reduced with the change of large agglomerate grains to smaller separate sphere grains after current passage. This is confirmed by an increase in the electrolyte resistance under cathodic current treatment (shown in Fig. 3a). If the porosity of the electrode remains constant, however, the smaller separate sphere grains in contact with the YSZ electrolyte may enlarge the three-phase boundary (electrolyte|electrode|gas, TPB) for oxygen reduction.

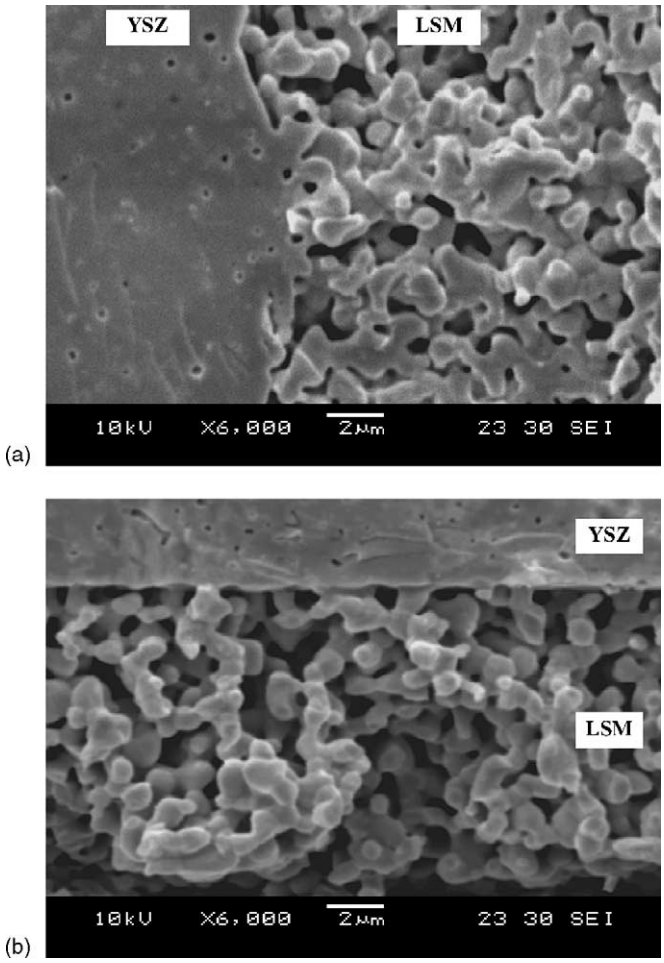

Fig. 2. Cross-section of YSZ|LSM half cell. (a) Newly prepared LSM electrode; (b) after cathodic current treatment of 120 min.

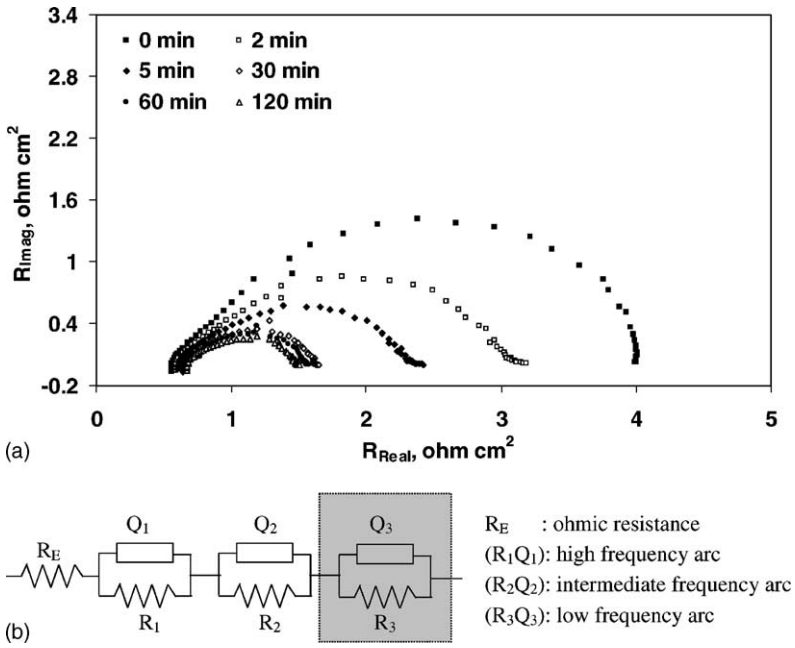

Fig. 3. (a) Impedance spectra of newly prepared LSM electrode as function of cathodic treatment time at 850 °C; (b) equivalent circuit of electrode reactions.

3.2. Polarization behaviors of newly prepared LSM electrode

Impedance measurements of the LSM electrode were carried out in the three-electrode system shown in Fig. 1. The polarization of the LSM electrode was interrupted periodically to obtain impedance spectroscopy. The impedance responses of a newly prepared LSM electrode measured at different interruption times when the electrode was polarized at a constant 0.3 A cm^{-2} at 850 °C in air are shown in Fig. 3a. Within the first few minutes of cathodic current passage, however, the resistance drops significantly and tends to be stable after 30 min of current passage. The resistance decreases from 3.38 Ω cm^2 for a newly prepared LSM electrode to 0.93 Ω cm^2 after 30 min, and finally to 0.72 Ω cm^2 after 120 min.

The impedance spectra were evaluated by the equivalent circuit shown in Fig. 3b, where R_E is the ohmic resistance between the reference electrode and LSM electrode, and (R_1Q_1), (R_2Q_2) and (R_3Q_3) correspond to the high-, intermediate- and low-frequency arcs, respectively. The low-frequency arc (R_3Q_3) normally appears when the oxygen partial pressure is lower than 0.1 atm. In this case, only low- and intermediate-frequency arcs can be observed in the impedance spectra measured in air. The values of R_E, R_1, R_2, R_3 and the constant-phase elements can be obtained through fitting the impedance spectra to the proposed equivalent circuit.

It should be noted that the cathodic current treatment has almost no effect on the high-frequency arc of the impedance spectra, but has a significant effect on the low-frequency arc. The enhancement of LSM electrode performance under cathodic current/potential treatment has also been reported by other workers [10,17]. Jiang et al. [10] and Lee et al. [18] reported that when the cathodic potential is sufficiently negative, the reduction of LSM electrode, e.g. the partial reduction of Mn^{3+} to Mn^{2+}, can occur with concomitant generation of oxygen vacancies according to:

$$O^x_{O,LSM} + 2Mn^{3+} + V_{\ddot{O},YSZ} + 2e^- \rightarrow V_{\ddot{O},LSM} + 2Mn^{2+} + O_{\ddot{O},YSZ} \quad (1)$$

Although an increase of the oxygen vacancies on the LSM surface is known to be the cause of the electrode enhancement, discrepancies are found in the literature about the mechanisms of enhancement of LSM electrochemical activity under cathodic potential/current treatment. Horita et al. [19] studied the LSM|YSZ interface by secondary-ion mass spectrometry and attributed the enhancement of the LSM electrode under cathodic current/potential treatment to the surface diffusion of oxygen vacancies on the LSM surface, which extends the active reaction sites from TPB to the bulk LSM surface for the electrochemical reduction of oxygen. Lee et al. [18] assumed that the low-frequency arc was due to a charge-transfer reaction. If it is so, the extension of reaction sites would increase the double-layer capacitance under cathodic current/potential treatment. As shown in Fig. 4, however, although the electrode polarization resistance is reduced by around five-fold after 120 min of cathodic current treatment, the constant-phase element of (R_2Q_2) remains virtually unchanged under cathodic current treatment. The independence of Q_2 on the cathodic treatment

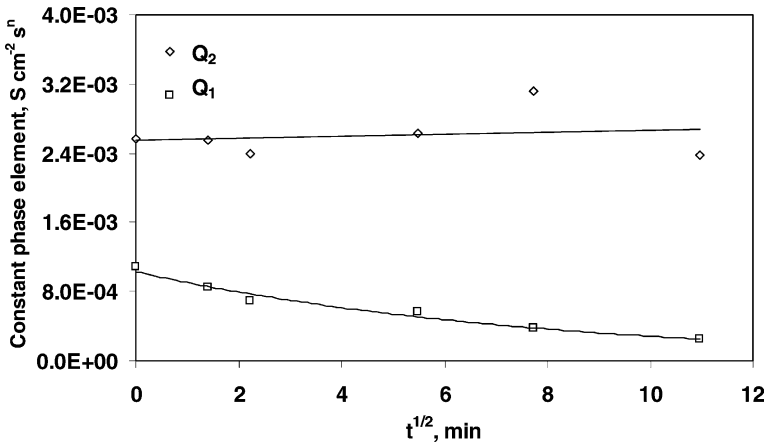

Fig. 4. Constant-phase element as function of cathodic treatment time at 850 °C.

rules out the possibility that the electrode process associated with (R_2Q_2) could be the charge transfer for oxygen reduction on LSM electrode surface. Another explanation for the improvement in electrochemical activity of the LSM electrode under cathodic treatment is that the generation of oxygen vacancies on the LSM surface enhances the surface diffusion oxygen species from reaction sites to the TPB [11,20].

If the impedance is measured in the same LSM electrode with same measurement conditions, the distance of the double layer and the dielectric constant may be assumed to be constant and the double-layer capacity can be used to predict the coverage of electrode on the electrolyte. As shown in Fig. 4, the constant-phase element of (R_1Q_1) decreases slightly with the cathodic treatment time, which corresponds to increase in electrolyte resistance and changes in the LSM electrode microstructure. This supports the conclusion that the reaction processes at the high-frequency arc (R_1Q_1), are related to the contact region between the LSM electrode and the YSZ electrolyte surface, which is reduced under cathodic current treatment.

3.3. Impedance spectra as a function of dc bias

The impedance responses of a LSM electrode under an applied cathodic dc bias at 850 °C in air are shown in Fig. 5. Two semi-circles can be clearly observed and the polarization impedance of the electrode decreases with increase in the applied bias. Liu and Wu [21] have suggested that reaction process will be an electrochemical, not a pure chemical, step if the impedance reduces under an applied dc bias. Nevertheless, this is not true if the overall reaction involves a series of elementary reaction processes, which include electrochemical and chemical steps. Because the elementary processes are associated with each other during reaction (v.i.), any elementary process, whether be it electrochemical or chemical, can exhibit the general Butler–Volmer relation. In fact, the dependence of Q_1 and Q_2 on the dc bias rules out the possibility that the reaction processes associated with (R_1Q_1) and (R_2Q_2) are charge-transfer steps (shown in Fig. 6). If a reaction process is a charge-transfer step, its double-layer capacity should be independent of the dc bias. The dependence of capacity (or constant-phase element)

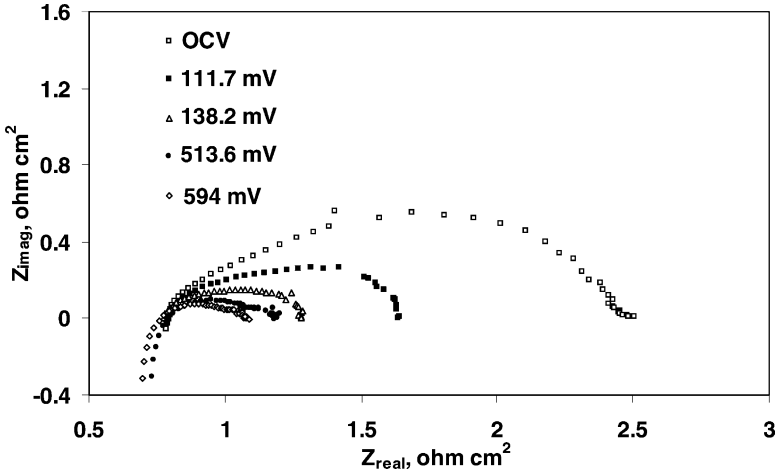

Fig. 5. Impedance responses of LSM electrode as function of dc bias.

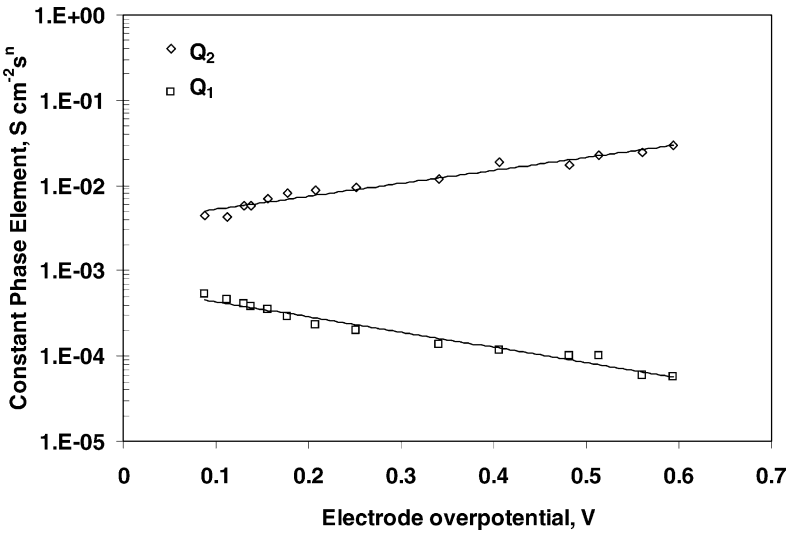

Fig. 6. Effect of dc bias on constant-phase element of high- and low-frequency arcs.

on the dc bias suggests that the oxygen reduction may involve chemical or physical processes at the LSM electrode surface.

Under a high current, the YSZ electrolyte may be decomposed to form suboxide (ZrO_{1-x}), which is an electronic conducting phase [22]. The high polarization may also lead to partial reduction of Mn^{3+} to Mn^{2+} with concomitant generation of oxygen vacancies [10,18]. This will reduce the dielectric constant, and increase the distance of the double-layer at the electrode|electrolyte interface. Consequently, capacitance of the high-frequency arc, Q_1, increases with increase in electrode polarization. The reason for the dependence of Q_2 on electrode polarization is still unclear. It may be due to the faster surface diffusivity of oxygen intermediate species at the LSM surface under higher polarization conditions.

3.4. Impedance spectra as a function of temperature and oxygen partial pressure

Before impedance measurements were conducted, a cathodic current of 300 mA cm^{-2} was applied at the LSM electrode for 120 min. The impedance spectra of the LSM electrode as a function of temperature and oxygen partial pressure p_{O_2} were investigated over the temperature range 700–950 °C and at oxygen partial pressures from 0.001 to 1 atm.

The impedance spectra measured at 850 °C and over an oxygen partial pressure range of 0.001–1 atm are presented in Fig. 7. Two depressed arcs can be observed at oxygen partial pressures of 0.21 and 1 atm. At low oxygen partial pressures, e.g. 0.01 and 0.001 atm, a new arc appears at low frequency (R_3Q_3). This means that the rate-determining

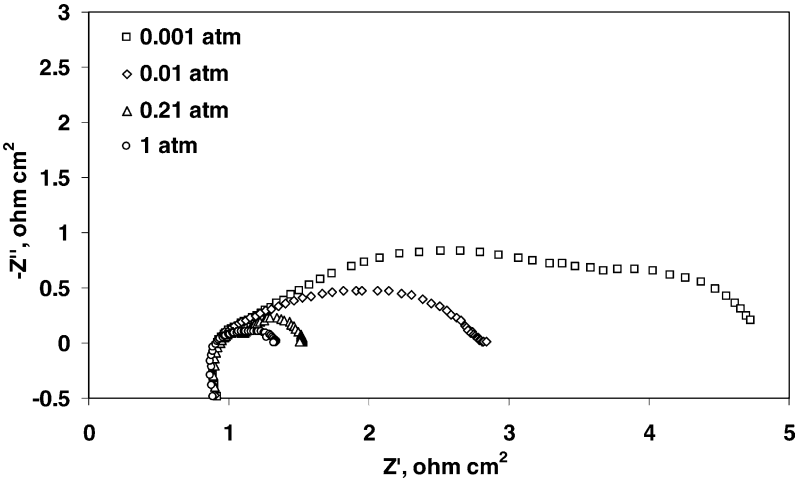

Fig. 7. Dependence of oxygen partial pressure on impedance spectra of LSM electrode at 850 °C.

Table 1
Dependence (R_1Q_1), (R_2Q_2) and (R_3Q_3) on p_{O_2} obtained from EIS responses of pure LSM electrode

Temperature (°C)	m in $1/R_1 \propto p_{O_2}^m$	m in $1/R_2 \propto p_{O_2}^m$	m in $1/R_3 \propto p_{O_3}^m$
750	0.003	0.25	–
800	0.02	0.268	0.96
850	0.01	0.276	0.97
900	0.02	0.263	1.02

steps of oxygen reduction at a LSM|YSZ interface involve three or more elementary processes at low oxygen partial pressures. The values of R_1, R_2 and R_3 can be obtained through fitting the impedance spectra to a proposed model. The p_{O_2}-dependence of the high-, intermediate- and low-frequency arcs of the LSM electrode is summarized in Table 1. At 800 °C, it is found that $1/R_1$ is independent of the oxygen partial pressure, while $1/R_2$ and $1/R_3$ are approximately proportional to $p_{O_2}^{0.268}$ and $p_{O_2}^{1.02}$, respectively. This relationship is consistent with the results reported by Kim et al. [8] for a LSM|YSZ composite electrode. Published results show other dependence of $p_{O_2}^x$ on $1/R_2$, i.e. x ranges from 0.14 to 0.3 [23] and 0.5 [15]. The difference may be due to the overlapping of the intermediate-frequency arc with the high-frequency arc ($x \leq 0.25$) or with the low-frequency arc ($x \geq 0.25$).

A Bode plot of the LSM electrode at various temperatures with an oxygen partial pressure of 0.001 atm is shown in Fig. 8. The purpose of such experiments is to study the effect of temperature on peak frequency of each frequency arc. It is found that the peak frequency of the low- and high-frequency arcs (R_1Q_1) and (R_3Q_3) is independent of temperature. Because the peak frequency is equal to the inverse of the resistance times the capacity, the summit frequency of the intermediate arc (R_2Q_2), increases with increase in temperature, which results in a weaker dependence of the capacitance on the temperature than for the low- and high-frequency arcs.

By fitting the impedance curves using the equivalent-circuit model shown in Fig. 3b, the respective temperature dependence of R_1, R_2 and R_3 is obtained and plotted in Fig. 9. The activation energy of R_1 is about 107 kJ mol^{-1} and is close to that of the conductivity of a 8 mol% yttria stabilized zirconia electrolyte, and is lower than 156 kJ mol^{-1} for R_2. Jiang et al. [13] reported corresponding activation energies of 109 and 163 kJ mol^{-1} in the presence of a chromia-forming alloy for the high-frequency arc [13]. The high value of R_1 in the presence of chromia-forming alloy is probably related to the high activation energy (i.e. 230 kJ mol^{-1}) for oxygen ion diffusion in Cr_2O_3. The independence of (R_1Q_1) on p_{O_2}, suggests that neither atomic oxygen nor molecular oxygen is involved in the reaction process [24–26]. As discussed earlier, the dependence of Q_1 on electrode polarization and cathodic treatment time shows that electrode processes at the high-frequency arc are not charge transfer. It can be concluded that the reaction processes at the high-frequency arc could be the migration and incorporation of oxygen ions from the TPB into the YSZ electrolyte lattice), i.e.

$$O^{2-}_{TPB,LSM} + V_{\ddot{O},YSZ} \Rightarrow O^{x}_{O,YSZ} \quad (2)$$

To clarify which reaction processes contribute to the low-frequency arc, impedance spectra of LSM electrode were obtained under different gas mixtures (O_2 balanced by He and N_2, respectively). The effect of balance gas on the impedance spectra at 900 °C with an oxygen partial pressure of 0.001 atm is shown in Fig. 10. At the same oxygen partial pressure, a different balance of gases affects only the low-frequency arc. Because the effective diffusion coefficient of oxygen is different in this situation, it is reasonable to attribute the low-frequency arc to a gas-diffusion step. Actually, a $p_{O_2}^{1.02}$ dependence of $1/R_3$ also indicate that the low-frequency arc may be related to the gas diffusion of oxygen from the bulk to the reaction sites though the porous LSM electrode.

Given the results discussed in Sections 3.2 and 3.3, the variation of the intermediate-frequency arc (R_2Q_2) under

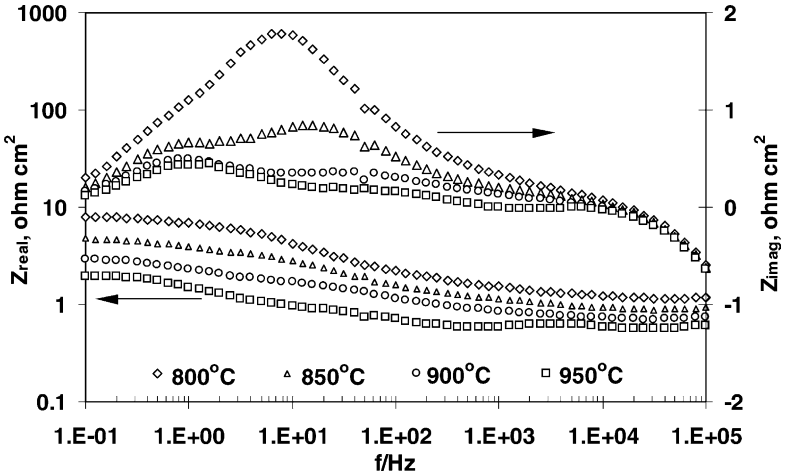

Fig. 8. Impedance spectra of LSM electrode at various temperatures ($p_{O_2} = 0.001$ atm, N_2 balance).

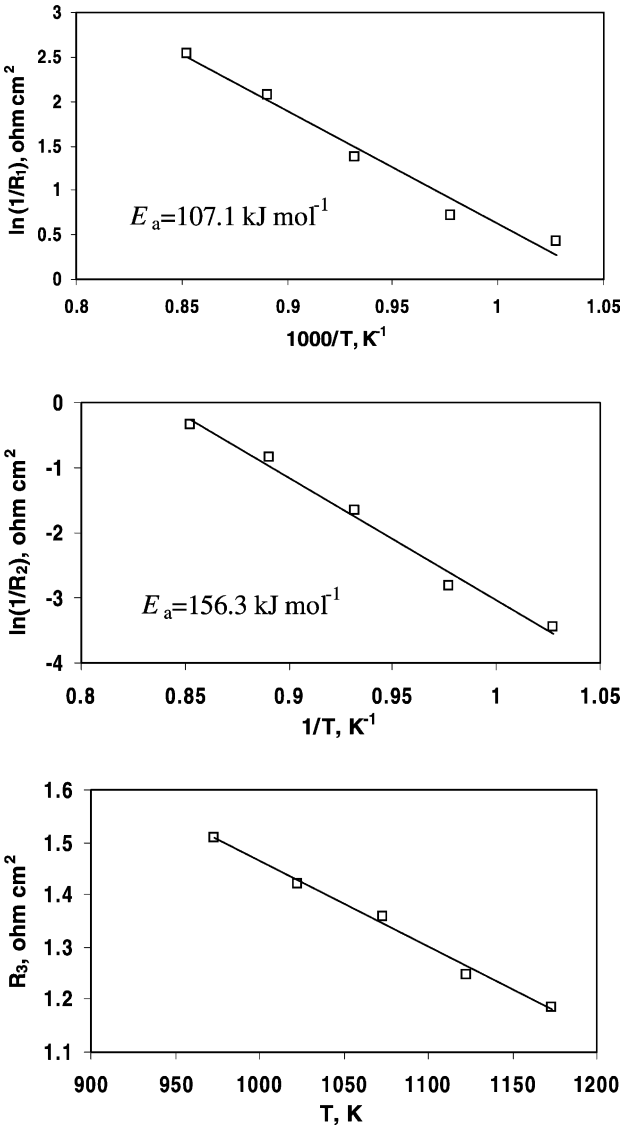

Fig. 9. Temperature dependence of R_1, R_2 and R_3 for oxygen partial pressure of 0.001 atm.

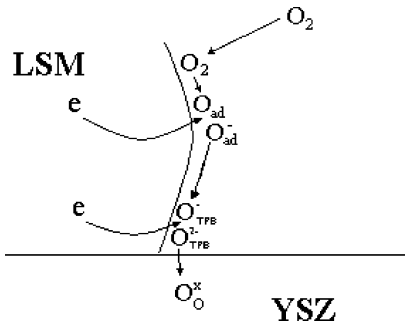

Fig. 11. Schematic of oxygen reduction path on LSM electrode.

cathodic polarization suggests that the reaction processes could not be charge-transfer, but are the dissociation and surface diffusion of oxygen intermediate species on the LSM surface. Although various oxygen intermediate species have been reported [8,12], a possible oxygen reduction path at the LSM|YSZ interface is shown in Fig. 11. At least six elementary steps may be involved in the oxygen reduction processes, as follows.

Step 1 $O_2(\text{bulk}) \rightarrow O_2(\text{interface})$

Step 2 $O_2(\text{interface}) \rightarrow 2O_{ad}$

Step 3 $O_{ad} + e^- \rightarrow O_{ad}^-$

Step 4 $O_{ad}^- \rightarrow O_{TPB}^-$

Step 5 $O_{TPB}^- + e^- \rightarrow O_{TPB}^{2-}$

Step 6 $O_{TPB,LSM}^{2-} + V_{\ddot{O},YSZ} \Rightarrow O_{O,YSZ}^{x}$

The rate equations corresponding to each elementary reaction step can be written as:

$$r_1 = k_1 p_{O_2,\text{bulk}} - k_{-1} p_{O_2,\text{interface}} \quad (3)$$

$$r_2 = k_2 p_{O_2,\text{interface}} - k_{-2} a_{O_{ad}}^2 \quad (4)$$

$$r_3 = k_3 a_{O_{ad}} e^{-fE/2} - k_{-3} a_{O_{ad}^-} e^{fE/2} \quad (5)$$

$$r_4 = k_4 a_{O_{ad}^-} - k_{-4} a_{O_{TPB}^-} \quad (6)$$

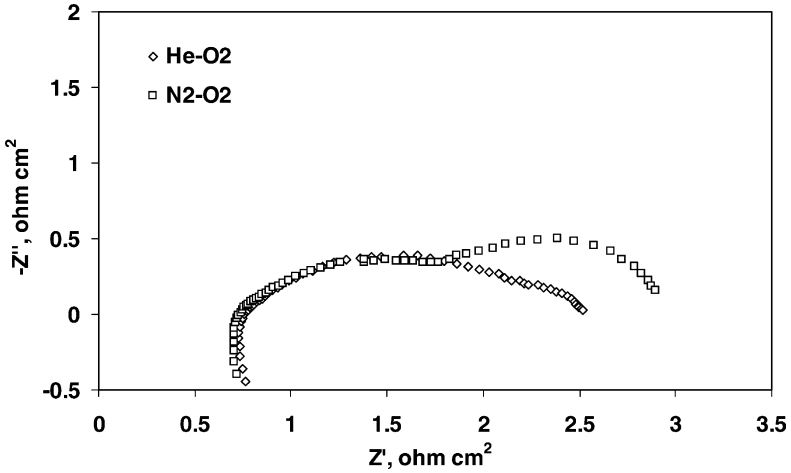

Fig. 10. Impedance spectra of LSM electrode with different balance gases ($T = 900\,^\circ\text{C}$, $p_{O_2} = 0.001$ atm).

$$r_5 = k_5 a_{O^-_{TPB}} e^{-fE/2} - k_{-5} a_{O^-_{TPB}} e^{fE/2} \quad (7)$$

$$r_6 = k_6 a_{O^{2-}_{TPB}} - k_{-6} \quad (8)$$

where k_i and k_{-i} ($i = 1$–6) are temperature-dependant rate constants for the forward and backward reactions, respectively, and $f = F/RT$.

As discussed above, the rate determining steps for oxygen reduction could be gas diffusion, surface diffusion of oxygen intermediate species on LSM surface, and incorporation of oxygen ions into YSZ electrolyte lattice (e.g. steps 1, 4 and 6). If step 1 is the rate-determining step, steps 2–6 are treated as being virtually in equilibrium. Thus:

$$p_{O_2,\text{interface}} = \frac{k_{-2}}{k_2} a^2_{O_{ad}} \quad (9)$$

$$a_{O_{ad}} = \frac{k_{-3}}{k_3} a_{O^-_{ad}} e^{fE} \quad (10)$$

$$a_{O^-_{ad}} = \frac{k_{-4}}{k_4} a_{O^-_{TPB}} \quad (11)$$

$$a_{O^-_{TPB}} = \frac{k_{-5}}{k_5} a_{O^{2-}_{TPB}} e^{fE} \quad (12)$$

$$a_{O^{2-}_{TPB}} = \frac{k_{-6}}{k_6} \quad (13)$$

Substituting Eqs. (9)–(13) into Eq. (3) gives the steady-state reaction rate, which converts to a current ($i = -nFr$) as:

$$i_1 = i_{anode} - i_{cathode} = nFk_1 p_{O_2,bulk} - nFk_{-1} \frac{k_{-2}}{k_2} \left(\frac{k_{-3}k_{-4}k_{-5}k_{-6}}{k_3k_4k_5k_6} \right)^2 \exp(4fE) \quad (14)$$

Under equilibrium conditions, i_1 is equal to zero. Assuming:

$$i_{0,1} = nFk_1 p_{O_2,bulk} = k_{-1} \frac{k_{-2}}{k_2} \left(\frac{k_{-3}k_{-4}k_{-5}k_{-6}}{k_3k_4k_5k_6} \right) \exp(4fE_{eq}) \quad (15)$$

then, when step 1 is the rate-determining step, the net current through the LSM electrode in Eq. (14) can be rewritten as:

$$i_1 = i_{0,1}[\exp(4f\eta) - 1] \quad (16)$$

If step 4 is considered to be the rate-determining step, then steps 1–3, 5 and 6 are virtually in equilibrium. In the same manner described above, the expression of $i_{0,4}$ and i_4 can be written as:

$$i_{0,4} = nFk_4 \frac{k_3}{k_{-3}} \left(\frac{k_1k_2}{k_{-1}k_{-2}} \right)^{1/4} \times \left(\frac{k_{-3}k_{-4}k_{-5}k_{-6}}{k_3k_4k_5k_6} \right)^{1/2} p^{1/4}_{O_2,bulk} \quad (17)$$

$$i_4 = i_{0,4}[\exp(f\eta) - \exp(-f\eta)] \quad (18)$$

If step 6 is the rate-determining step, then steps 1–5 are virtually in equilibrium. The expression of $i_{0,6}$ and i_6, can be written as:

$$i_{0,6} = nFk_{-6} \quad (19)$$

$$i_6 = i_{0,6}[1 - \exp(-2f\eta)] \quad (20)$$

The dependence of $i_{0,1}$, $i_{0,4}$, and $i_{0,6}$, on p_{O_2} is found to be 1, 0.25 and 0, respectively, which corresponds to 1.02, 0.268 and 0.02 for $1/R_3$, $1/R_2$ and $1/R_1$ obtained at 800 °C for the LSM electrode. The good agreement between the analytical model and the experimental results further confirms that the proposed oxygen reduction processes at the LSM|YSZ interface are reasonable assumptions. It also should be noted that although the three assumed rate-determining steps are not the electrochemical steps (charge-transfer), the *V–I* relation satisfies the general Bulter–Volmer equation. That is why a reaction process cannot be judged electrochemical or chemical merely according to the Bulter–Volmer relation.

4. Conclusions

The oxygen reduction processes at the LSM|YSZ interface have been studied by impedance spectroscopy at different temperatures and oxygen partial pressures. The variation of the constant-phase element is used to determine whether the impedance frequency arc is an electrochemical or a chemical process. The independence of the constant-phase element on the cathodic treatment time rules out the reaction processes at the low-frequency arc to be charge-transfer steps. The good agreement between the theoretical analysis and the experimental results for the p_{O_2} dependence of i_0 on $1/R$ indicates that the proposed oxygen reduction model is reasonable. At least six elementary steps and three rate-determining steps are found to be involved in the oxygen reduction processes at the LSM|YSZ interface, e.g. gas diffusion through the porous LSM electrode from the bulk to the reaction sites, the surface diffusion of oxygen intermediate species along the LSM surface, and the incorporation of oxygen ions from the TPB into the YSZ electrolyte lattice.

References

[1] N.Q. Minh, T. Takahashi, Science and Technology of Ceramic Fuel Cells, Elsevier, Amsterdam, 1995.
[2] Y. Takeda, S. Nakai, T. Kojima, R. Kanno, N. Imanishi, G.Q. Shen, O. Yamamoto, M. Mori, C. Asakawa, T. Abe, Mater. Res. Bull. 26 (1991) 153.
[3] S.P. Jiang, J.G. Love, J.P. Zhang, M. Hoang, Y. Ramprakash, A.E. Hughes, S.P.S. Badwal, Solid State Ionics 121 (1999) 1.
[4] S.P. Jiang, J.P. Zhang, X.G. Zheng, J. Eur. Ceram. Soc. 22 (2002) 361.
[5] H. Kamata, A. Hosaka, J. Mizusaki, H. Tagawa, Solid State Ionics 106 (1998) 237.
[6] M.J. Jørgensen, S. Primdahl, C. Bagger, M. Mogensen, Solid State Ionics 139 (2001) 1.

[7] Y. Jiang, S.Z. Wang, Y.H. Zhang, J.W. Yan, W.Z. Li, Solid State Ionics 110 (1998) 111.
[8] J.-D. Kim, G.-D. Kim, J.-W. Moon, Y.-I. Park, W.-H. Lee, K. Kobayashi, M. Nagai, C.-E. Kim, Solid State Ionics 143 (2001) 379.
[9] H.Y. Lee, A study on electrochemical and interfacial properties of $La_{1-x}Sr_xMnO_3$ and $Y_{0.8}Ca_{0.2}Fe_xCo_{1-x}O_3$ cathode for SOFC, Ph.D. thesis, Seoul National University, South Korea.
[10] Y. Jiang, S.Z. Wang, Y.H. Zhang, J.W. Yan, W.Z. Li, J. Electrochem. Soc. 145 (1998) 373.
[11] E. Siebert, A. Hammouche, M. Kleitz, Electrochim. Acta 40 (1995) 1741.
[12] F.H. van Heuveln, H.J.M. Bouwmeester, F.P.F. van Berkel, J. Electrochem. Soc. 144 (1997) 1134.
[13] S.P. Jiang, J.P. Zhang, K. Foger, J. Electrochem. Soc. 147 (2000) 3195.
[14] M.J. Jørgensen, M. Mogensen, J. Electrochem. Soc. 148 (2001) A433.
[15] H. Kamata, A. Hosaka, J. Mizusaki, H. Tagawa, Solid State Ionics 106 (1998) 237.
[16] S.P. Jiang, J.G. Love, Solid State Ionics 158 (2003) 45.
[17] S.P. Jiang, J.G. Love, Solid State Ionics 138 (2001) 183.
[18] H.Y. Lee, W.S. Cho, S.M. Oh, J. Electrochem. Soc. 142 (1995) 2659.
[19] T. Horita, K. Yamaji, M. Ishikawa, N. Sakai, H. Yokokawa, T. Kawada, T. Kato, J. Electrochem. Soc. 145 (1998) 3196.
[20] B. Gharbage, T. Pagnier, A. Hammou, J. Electrochem. Soc. 141 (1994) 2118.
[21] M.L. Liu, Z.L. Wu, Solid State Ionics 107 (1998) 105.
[22] B.C. Nguyen, T.L. Lin, D.M. Mason, J. Electrochem. Soc. 133 (1986) 1807.
[23] M.J.L. Østergård, M. Mogensen, Electrochim. Acta 38 (1993) 2015.
[24] M.J. Jørgensen, S. Primdahl, M. Mogensen, Electrochim. Acta 44 (1999) 4195.
[25] S. Wang, Y. Jiang, Y. Zhang, J. Yan, W. Li, Solid State Ionics 113–115 (1998) 291.
[26] E.P. Murray, T. Tsai, S.A. Barnett, Solid State Ionics 110 (1998) 235.